Thin Solid Films 520 (2012) 1872–1879

Contents lists available at SciVerse ScienceDirect

Thin Solid Films

journal homepage: www.elsevier.com/locate/tsf

Layered and interfacially blended polyelectrolyte multi-walled carbon nanotube composites for enhanced ionic conductivity

Xianke Gu [a,b], Daniel B. Knorr, Jr. [a,c], Guojian Wang [b], René M. Overney [a,*]

[a] Department of Chemical Engineering, University of Washington, Seattle, WA 98115-1750, USA
[b] School of Materials Science and Engineering, Tongji University, Shanghai 200092, China
[c] Macromolecular Science and Technology Branch, United States Army Research Laboratory, Aberdeen Proving Ground, MD 21009, USA

ARTICLE INFO

Article history:
Received 28 June 2011
Received in revised form 9 September 2011
Accepted 9 September 2011
Available online 16 September 2011

Keywords:
Poly(ethylene oxide)
Poly(acrylic acid)
Layer-by-layer
Multi-walled carbon nanotubes
Polyelectrolyte
Ion conduction
Electrostatic force microscopy
Lateral force microscopy

ABSTRACT

To enhance the ionic conductivity in solid phase polyelectrolyte systems for lithium ion battery applications demands effective control of the phase properties. Here, we report on a strategy involving a layer-by-layer methodology of two polyelectrolytes, poly(ethylene oxide) (PEO) and poly(acrylic) acid (PAA) and carboxylic acid functionalized multi-walled carbon nanotubes (MWNTs). Optimization of the assembly strategy revealed that undoped and lithium-ion doped stacking of four layers provides excellent film growth and improvement of the ionic conductivity of up to 10^{-5} S cm^{-1}, which exceeds conventional assemblies of lithium-ion doped [PEO/PAA] by up to two orders of magnitude. Although ionic conductivity was most effectively enhanced for ultrathin films (<100 nm), [PEO/PAA/PEO/(PAA + MWNT)] stacking still provides an ionic conductivity of >10^{-6} S cm^{-1} for thick films (>2 μm). The improvement of ionic conductivity was attributed to (i) interfacial phase mixing (blending) of the two polyelectrolytes, (ii) the MWNT contribution in the interfacial region, and (iii) the preferential adsorption of lithium-ions along the carbon nanotubes. This study involved a series of scanning probe methods including lateral force microscopy, and electrostatic force microscopy.

© 2011 Elsevier B.V. All rights reserved.

1. Introduction

Thin flexible all-solid ("dry") polymer electrolytes (SPEs) show great technological potential for electrochemical devices, such as batteries [1,2]. Serving as hosts for complexing metal salts, dry SPEs eliminate the possibility of leakage and the production of combustible reaction products, and promise most of the benefits of current thin film polymer electrolytes from cost-effectiveness to shape versatility. The most notable drawback of dry SPEs, however, is their relative low ionic conductivity at room temperature, which is orders of magnitude (10^{-3} S cm^{-1}) from being of practical use for battery applications [3].

To date, one of the most promising material candidates for dry SPEs in solid-state batteries involving high molecular weight polymers is poly(ethylene oxide) (PEO) complexed with a variety of Li^+-ion salts [1,3]. However, PEO-Li ion based dry SPEs have only found commercialization in large systems [1], as ionic conductivities exceeding 10^{-4} S cm^{-1} could so far only be reached at the polymer melting point around 70 °C [3]. To enter the portable device market, hybrid polymer electrolyte systems were developed in which the polymer electrolyte served as a host material that was swollen with a liquid solvent and a salt, which led to the first practical (although not "dry") SPE commercialization by Bellcore [4].

Ionic transport in dry SPEs occurs predominantly through an association-dissociation between ions and the polymer host [5]. The sequential oxyethylene groups in the PEO backbone and its polar side groups are the main contributor in dissolving ionic salts to form polymer-salt complexes, typically expressed by the number of ether oxygens per mole of salt, *i*, i.e., PEO_i-salt [3]. It is usually perceived that fast ionic transport benefits from amorphous polymer phases in solid polymers [3,5]. As most polyelectrolytes are known to crystallize, various efforts from cross-linking [5–7], blending [8–10], plasticization [1,3], to incorporation of inorganic particles [11,12] have been undertaken to improve the mechanical stability (in particular concerning polymer gel electrolytes) and to suppress crystallization in dry SPEs, and thus, enhance the ionic mobility. In other words, dry SPE research has been predominantly directed towards the development of low glass transition polymer electrolyte hosts with large and stable amorphous phases. In this respect, embedding inorganic interfaces via fillers into the polymer matrix has been quite popular [13,14]. Often this approach has been described as a plasticizing effect that is also observed by either blending polymers or incorporating metal salts into the polymer matrix.

However, since Gadjourova et al.'s work [15], in which high ionic transport could be supported in an ordered crystalline environment, the specific role of the filler in promoting ionic transport is rather elusive, and raises questions about the impact of polymer ordering and

* Corresponding author.
E-mail address: roverney@u.washington.edu (R.M. Overney).

0040-6090/$ – see front matter © 2011 Elsevier B.V. All rights reserved.
doi:10.1016/j.tsf.2011.09.020

Samsung Ex. 1016, Page 1 of 8
Samsung Electronics Co., Ltd., et al. v. Molecular Rebar Design, LLC
IPR2025-00358

crystalline structures within interfacial regions of polymer composites. That interfacial constraints on the nanoscale indeed have a significant impact on the PEO crystalline structure has been addressed multiple times [16–18]. While Schonherr et al.[16] and Massa et al. [17] reported a reduction in the growth rates with decreasing film thickness for PEO films thinner than 250 nm, Wang et al. [18] just recently discovered crystalline phases in dimensionally-constrained (~20 nm) PEO systems that are structurally different from bulk systems. Considering the influential effect of interfaces on the polymer structure, Hammond's group [19] explored the impact of the layer-by-layer (LBL) assembly process on the ion conductivity involving PEO and poly(acrylic acid) (PAA) complexed with $LiCF_3SO_3$. This alternative process of rationally incorporating interfacial constraints into the design of dry SPEs yielded ionic conductivities on the order of 10^{-7} S cm^{-1} at room temperature under ambient conditions (52% relative humidity (RH)). Although this signifies a noteworthy improvement over the ~10^{-9} S cm^{-1} at 40 °C for $(PEO)_x-LiCF_3SO_3$, [3] it still remains too low for practical use.

Subsequent work by Hammond's group revealed hydrogen bonded complexes in the PEO/PAA LBL system with only one glass transition, leading to the conclusion of the formation of an amorphous true blend [20,21]. Polymer blending can significantly impact the ionic conductivity as shown by Baskaran et al. [9] with poly(vinyl acetate) (PVAc) and poly(methyl methacrylate) (PMMA) complexed with $LiClO_4$. They reported for these systems ionic conductivities of up to 10^{-3} S cm^{-1} at 30 °C [9], exceeding values of $(PEO)_x-LiClO_4$ (~10^{-7} S cm^{-1} at room temperature) [22] by four orders of magnitude. In contrast to Hammond's finding for PEO/PAA LBL systems, PVAc-PMMA blend systems revealed two glass transitions, which is an indication of the presence of internal interfaces. While Baskaran et al. [9] attributed the high ionic conductivity in PVAc-PMMA-$LiClO_4$ to the suppression of crystallinity alone, Zhou et al. [5] argued that the polar carbonyl groups also have to be considered, as they can increase the number density of charge carriers. Consequently, Zhou et al. explored dry SPE systems with flexible carboxyl side groups, in which the ionic dissociation of the lithium salts in the composite could be accelerated [5].

Our recent studies on the phase behavior in the sub-100 nanometer regime of PEO, and PEO and poly(acrylic acid) (PAA) LBL systems, and the ionic transport properties if complexed with $LiCF_3SO_3$, revealed, in correspondence to earlier findings [19], the crystalline phase suppression within the PEO phase [23]. Crystallization could not, however, be entirely eradicated for low stack numbers, revealing multiple in plane phases, consisting of a PEO-PAA blended dominating phase with largely non-crystalline PEO content, PAA rich regions, crystalline PEO domains, and also bulk-like PAA [23]. Interestingly, this highly heterogeneous thin film (~<100 nm) LBL growth regime was found to exceed the ion conductivity of bulk $(PEO)_x-LiCF_3SO_3$ systems by up to 2 orders in magnitude at 40 °C.

In summary, current efforts towards ionic conductivity enhancement in dry SPEs have focused predominantly on providing mobility to the polymer segments, and increasing the dissociation of lithium slats in the composite. Materials of choice have been polymer blends and high dielectrics. Various strategies have been explored to enhance the ionic conductivity in polymer electrolyte films, such as embedding nanofillers into the polymer matrix [13,14,24]. One of these nanofillers in particular, i.e., carbon nanotubes (CNTs), have prompted intensive studies, because of their exceptional electronic properties [25,26]. Ionic conductivity enhancements of up to ~10^{-8} S cm^{-1} and ~10^{-5} S cm^{-1} have been achieved with 15 wt.% CNT fillers in PEO [27] and 2 wt.% CNT fillers in PEO-LiClO4(8:1) electrolytes [28], respectively. However, in the latter case, very high atomic lithium loadings (~1.5 wt.%) were required[28]. It was argued that the very high aspect ratio of the carbon nanotubes when compared to spherical particles is responsible for long-range disorder in the polymer matrix [28], which may aid in preserving an amorphous structure for PEO. A combined nanofiller particle-LBL strategy for further enhancement of the ionic conductivity may be achieved by embedding plasticizing and electric transport enhancing particles, such as CNTs, in one of the LBL stack components [29,30]. Such CNT-polymer films can avoid short circuits due to the fact that CNTs do not contact each other directly, resulting in limited or no electronic transport.

In this paper, we supply water soluble multiwall carbon nanotubes to PEO/PAA LBL films. The objective is to inject multi-walled carbon nanotubes (MWNTs) into the blend interphase region of the binary polyelectrolyte system, which is known to form for PAA and PEO during the LBL assembly process [20,23], in order to maintain the beneficial hydrogen bonding effects of PAA that reduce PEO crystallization [21] and, at the same time, mitigate the relatively poor conductivity of PAA. Further, we demonstrate the direct measurement of the blend interphase from ultrathin films to bulk films by lateral force microscopy (LFM) and electrostatic force microscopy (EFM), which provides insight into the growth mechanism of the tri-component LBL film. The tri-component film with and without added lithium triflate appears to provide a pathway for ion transfer, yielding PAA-rich blend regions with higher ionic conductivity than those without MWNTs.

2. Experimental section

2.1. Materials and sample preparation

Nonionic PEO (4000 kM_w, Polysciences) and polyanionic PAA (90 kM_w, 50 wt.% water solution, Carbemer Inc.) were used as received. The polymers were weighed and dissolved in Millipore Milli-Q filtered water (18 MΩ·cm), and the resultant solutions were pH adjusted to a pH of 2.5 with dilute aqueous HCl. The PEO solution was stirred for 24 h to ensure complete dissolution. All polymer solutions were 0.020 M (polymer concentrations with respect to repeat unit).

Multiwalled carbon nanotubes (MWNT) prepared by a conventional CVD method (>95% purity, length 10–20 μm, outer diameter 30–50 nm, Cheaptubes, Inc.) were refluxed in concentrated H_2SO_4/HNO_3 (3/1 v/v, 96% and 70%, respectively) at 70 °C to form carboxylic acid functionalized MWNTs. The reaction product was then washed with water several times using a Teflon membrane filter with a pore diameter of 0.2 μm. MWNT powder was obtained from drying at 70 °C in vacuum for 24 h. For the final LBL MWNT containing solution, 10 mg of MWNT were dispersed in 20 ml of 0.02 M PAA solution and 20 ml water.

Indium-doped tin oxide (ITO) coated glass csubstrates (15 mm × 15 mm from Thin Film Devices, Inc.) were used as LBL substrates. ITO film resistance was measured to be 100 Ω/square. The ITO substrates were cleaned by ultrasonication (Model 08849, Cole-Parmer instrument company) in a series of solvents for 15 min each, in the following order: acetone, methanol, and water. Following the water cleansing, the substrates were dried under a jet of desiccated nitrogen gas. Immediately before use, the ITO glass substrates were cleaned in UV for 20 min.

In a typical assembly, an ITO coated glass substrate was immersed for 10 min in PEO (0.020 M H_2O solution), followed by a 10 minute immersion into PAA (0.020 M H_2O solution), then another 10 min back into PEO, and finally, 10 min in the LBL MWNT-PAA solution described above. After each step, the sample was rinsed for 2 min, 1 min, and then 1 min in 3 separate water beakers. This sequence (referred in the following as a stack) after being repeated m times produced a $[PEO/PAA/PEO/(PAA+MWNT)]_m$ (note: m is used for system with 4 repeating stacks, while n is used for system with 2 repeating stacks) composite film. Also, purely polymeric PEO/PAA control stacks were prepared following the same sequence except that every MWNT layer was replaced with a PAA layer. The same total number of layers was assembled for comparison. After assembly, all films were dried at 110 °C for 24 h, which has been shown to

Samsung Ex. 1016, Page 2 of 8
Samsung Electronics Co., Ltd., et al. v. Molecular Rebar Design, LLC
IPR2025-00358

effectively remove water from LBL assembled films [31]. Salt ions were implanted into some films by soaking the films after storage in aqueous solutions of $LiCF_3SO_3$, lithium triflate (LiTrif), that had been adjusted to pH 2.5. Soaking was done for 24 h, and films were dried without further rinsing under desiccated nitrogen immediately afterward [19].

2.2. Characterization

Scanning force microscopy (SFM) was employed to evaluate the topological information of the films. SFM was conducted with a scanning probe microscope (Topometrix Explorer, Veeco, CA) with contact mode cantilever sensors (PPP-CONT, Nanosensors, nominal and lateral spring constants of ~0.2 N/m and 80 N/m, respectively). Electrostatic force microscopy (EFM)[32] (diCaliber, Veeco, CA) and lateral force microscopy (LFM)[33] (Topometrix Explorer, Veeco, CA) were used to explore material phase heterogeneities to identify material components. Prior to friction coefficient measurements, the LFM cantilever was calibrated according to a well established method [34]. Film thicknesses were determined via a contact mode operated SFM (EasyScan 2, Nanosurf AG, Switzerland) of razor blade scratched films, a method that has been verified with profilometry involving thicker films. After assembly, 220 nm thick gold electrodes were deposited on the surface of the sample with an Angstrom gold deposition system. This process created two-electrode 3.14 mm^2 test beds in which the LBL assembled film were sandwiched between ITO and gold electrodes. The substrate dimensions allowed 16 such cells per substrate.

Ionic conductivity was evaluated by impedance spectroscopy, which was performed using an HP 4192A LF impedance analyzer (5 Hz to 10 MHz). The signal amplitude was 100 mV excluding the bias. Conductivity measurements were conducted in an environmental chamber at approximately 50% relative humidity. Impedance data of materials that have capacitive and resistive components, when represented in the Nyquist diagram (i.e., the negative of the imaginary part ($-\mathrm{Im}\,Z$) in the y axis and the real part ($\mathrm{Re}\,Z$) in the x axis —each point corresponding to a different frequency), lead to a succession of semicircles. The observed response was modeled by an equivalent circuit [21,35] consisting of two parallel elements, R_m (the resistance of the LBL film) and C_m (the LBL film capacitance), in series with two other parallel elements, R_p (the charge transfer resistance at the electrodes), and C_p (the capacitance of the double layer at the electrodes). The second intercept of the high frequency semi-circle with the real axis is the resistance (R_m) of the film. Hence, the conductivity (σ_b) is written

$$\sigma_b = 1/R_m \times l/A, \tag{1}$$

where l is the thickness and A is the area of the electrode deposited on the sample [36].

3. Results and discussion

3.1. Assembly strategy for film growth

Any effective fabrication method for practical applications has to be scaleable. For LBL approaches, as presented here, this requires effective material transfer during each dipping cycle. To determine an acceptable assembly strategy, five LBL assemblies were tested. The first assembly involved PEO and PAA only served as a control, and is referred to as $[PEO/PAA]_n$, where n identifies the number of binary stacks. Here, as in our previous work, the thickness of $(PEO/PAA)_n$ stacked LBL films revealed exponential growth up to a stacking number of $n = 8$, followed by linear growth [23]. The second set of binary stack systems entailed carboxylic functionalized carbon nanotubes (MWNT) dissolved prior to the LBL assembly in either the PEO or PAA phase, i.e., $[(PEO + MWNT)/PAA]_n$, and $[PEO/(PAA + MWNT)]_n$,. In the third assembly, MWNT were supplied separately as a film stack component in the stack sequence $[PEO/PAA/PEO/MWNT]_m$. The index m indicates here the numbers of layers in a quaternary stack system. Finally, MWNT were supplied within an additional PAA layer, i.e., within the stack sequence $[PEO/PAA/PEO/(PAA + MWNT)]_m$. The expansion to tri-stack-components was motivated by the results discussed below, but also by Kotov's LBL stacking of PAA, poly(ethyleneimine) (PEI), and a+-montmorillonite (MTM) nanoparticles (i.e., [PEI/PAA/PEI/MTM]), which showed rapid growth, affording fast preparation of nanostructured materials [37].

At first, the binary stack sequence $[(PEO + MWNT)/PAA]_n$ seemed to be the logical choice. However, the experiment showed that MWNTs settle out of the PEO solution. The second MWNT binary system, $[PEO/(PAA + MWNT)]_n$, produced only very thin films compared to the control $[PEO/PAA]_n$, Fig. 1, indicating an undesired polarity change in the PAA-MWNT stack component. An improvement with regard to film quality and material transfer was obtained by supplying MWNTs separately, Fig. 1. However, the best transfer performance of any MWNT system was obtained in the $[PEO/PAA/PEO/(PAA + MWNT)]_m$ stack sequence, also shown in Fig. 1, which compared favorably with the PEO/PAA control. $[PEO/PAA/PEO/(PAA + MWNT)]_m$ showed exponential growth early on (up to about $n = 10$), and then linear growth from that point on, which was similar to the growth of other polyelectrolyte multilayers [38]. If compared to current work in the literature, $[PEO/PAA/PEO/(PAA + MWNT)]_m$ surpasses the stack-layer growth for numerous other polymer-CNT LBL systems [39,40], as well as all other CNT LBL systems [29,41]. Compared to $[PEO/PAA]_n$ and $[PEO/(PAA + MWNT)]_n$, the growth thickness vs. layer number of $[PEO/PAA/PEO/(PAA + MWNT)]_m$ is not merely the sum of the two former systems. This suggests that a foundational PEO/PAA layer is required for incorporation of carbon nanotubes.

3.2. Ion-conductivity in MWNT LBL assemblies

Conductivity data is presented for direct comparison of $[PEO/PAA]_n$ and $[PEO/PAA/PEO/(PAA + MWNT)]_m$ in Fig. 2(a) and (b), in terms of thickness with and without Li Trif present, respectively. Clearly, ionic, rather than electrical, conductivity is supplied by the fact that the addition of Li Trif positively affects the conductivity, as shown in Fig. 2(b). The first striking observation in Fig. 2 is the high ionic conductivity in the ultrathin film region, which, according to our previous work [23] is dominated by PEO for $[PEO/PAA]_2$ [23]. The drop from ~10^{-7} S cm^{-1} for $[PEO/PAA]_2$ (thickness = 17 nm) by two orders of magnitude to 10^{-9} S cm^{-1} for a 10 stack system (thickness = 495 nm), Fig. 4(a), originates from the fact that, based

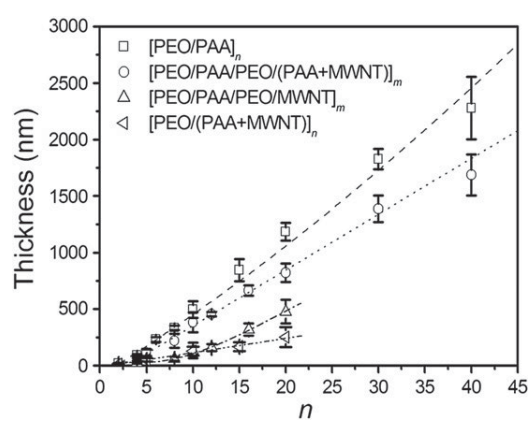

Fig. 1. Compilation of the film thickness evolution as a function of the layer stack number n, determined by SFM. For $[PEO/PAA/PEO/(PAA + MWNT)]_m$ and $[PEO/PAA/PEO/MWNT]_m$, $n = m/2$ for appropriate transfer comparison.

Samsung Ex. 1016, Page 3 of 8
Samsung Electronics Co., Ltd., et al. v. Molecular Rebar Design, LLC
IPR2025-00358

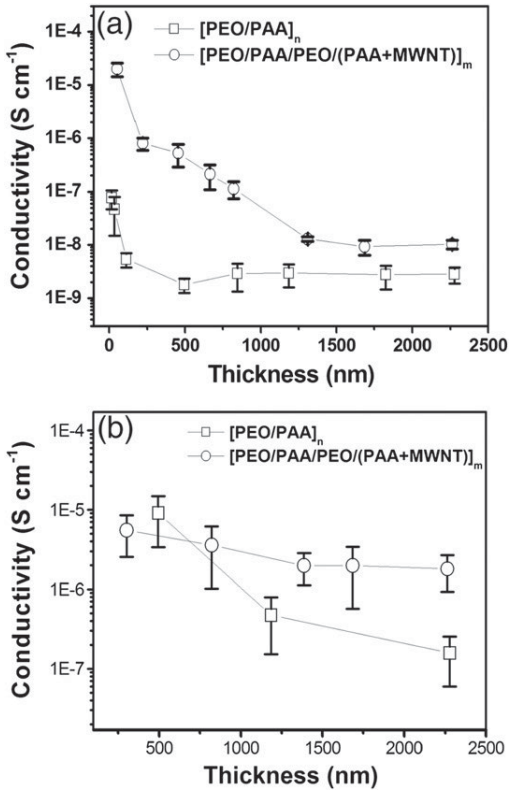

Fig. 2. Ionic conductivity vs. film thickness for PEO/PAA system and PEO/PAA/PEO/(PAA + MWNT) system at 48%–56% RH and 25 °C: (a) films without lithium triflate and (b) films soaked in lithium triflate solution with pH 2.5 for 24 h.

on our prior work [23], the PAA phase, which is a poor electrolyte, provides a more or less uniform surface coverage for $n>10$. The conductivity reaches a thickness independent limit of 10^{-9} S cm^{-1}, which is also in good correspondence with the literature of $n=30$ stacks at 53% RH and 25 °C, Table 1 [21]. [PEO/PAA/PEO/(PAA + MWNT)]$_m$, if compared to [PEO/PAA]$_2$, shows two significant enhancements (Fig. 4(a)). First, it raises the ion conductivity by more than two orders of magnitude to above 10^{-5} S cm^{-1} in the ultrathin film region, and second, it expands the interfacial effect seven fold from ~0.25 μm thick films to ~1.75 μm thick films.

As addressed above, ion-conductivity in polyelectrolyte systems is significantly enhanced by the addition of ions. To investigate the effect of the MWNT assembly on ion doping, we exposed [PEO/PAA]$_n$ and [PEO/PAA/PEO/(PAA + MWNT)]$_m$ film stacks to $LiCF_3SO_3$ 2.5 pH solutions. The ionic conductivity results are presented in Fig. 4(b). Ionic conductivity of [PEO/PAA]$_n$ LiTrif ranged from above ~10^{-5} to below ~10^{-7} S cm^{-1} as the thickness ranged from 495 nm to 2280 nm, which corresponds to $n=10$ and $n=40$ stacks, respectively. The conductivity at $n=40$ stacks is in good correspondence with literature values [21] of $n=30$ stacks at 53% RH and 25 °C, Table 1. The conductivities of [PEO/PAA/PEO/(PAA + MWNT)]$_m$ LiTrif exhibit values of 10^{-5}–10^{-6} S cm^{-1} as the thickness ranged from 383 nm to 2263 nm, corresponding to $m=5$ to 25. As previously mentioned, conductivities of ~10^{-5} S cm^{-1} have been achieved earlier with 2 wt.% CNT fillers in PEO-$LiClO_4$(8:1) electrolytes [28]. However, these systems required atomic lithium loadings of ~1.5 wt.% that exceed by about an order of magnitude the 0.1–0.3 wt.% range used here.

In accordance with the literature [19], the ion conductivity for [PEO/PAA]$_n$ LiTrif increased substantially by an order of magnitude relative to the undoped sample. Also, the interfacial effect was extended to a film thickness of over 2 μm. A more dramatic effect concerning the conductivity decay with film thickness occurred for the LiTrif doped [PEO/PAA/PEO/(PAA + MWNT)]$_m$ stack assembly. It dropped by less than half an order of magnitude over a film thickness regime of 2.5 μm, yielding an ionic conductivity of more than 10^{-6} S cm^{-1} in thick films, which are compared in Table 1 to literature values. All in all, bulk [PEO/PAA/PEO/(PAA + MWNT)]$_m$ without and with LiTrif multilayers possess limiting ionic conductivities of ~10^{-8} S cm^{-1} and 10^{-6} S cm^{-1} at 48–56% RH, which are 10 times higher than neat [PEO/PAA]$_n$ (~10^{-9} S cm^{-1}) and [PEO/PAA]$_n$ with LiTrif (~10^{-7} S cm^{-1}), respectively.

Previous work has shown that segmental motion assists diffusion of Li^+ in the PEO matrix [1]. The mobility of the Li^+ is related to the motions of the complexing segments of the PEO chain. Thus, the cation transport is described as the motion of the Li^+ species between complexation sites assisted by the segmental motion of the PEO matrix [42]. It has to be noted that Li^+ transport is faster in PEO compared to PAA, and the Li^+ charge carrier concentration increases with MWNTs present, as Li^+ ions prefer adsorbing at the MWNT walls [43]. Thus, MWNTs offer an effective ion transport bridge in [PEO/PAA/PEO/(PAA + MWNT)]$_m$, an aspect that is lacking in the [PEO/PAA]$_n$ control system.

3.3. Structure analysis of tri-component LBL films

3.3.1. Lateral force microscopy (LFM) analysis

To further elucidate the role of MWNTs in ionic conductivity, the films were analyzed locally based on their phase heterogeneities, mechanical and electronic properties by lateral force microscopy (LFM) and electrostatic force microscopy (EFM). [PEO/PAA/PEO/(PAA + MWNT)]$_m$ films revealed multiple phases at the free surface after the last deposition of PAA + MWNTs, as shown in the friction contrast images of Fig. 3. As shown, two phases can be discerned, the polymer phase and the carbon nanotubes, which are apparent due to the huge difference in friction coefficient between these phases. The darkest features are, based on their shape, attributed to carbon nanotubes, which have the lowest friction coefficient. The bulk phase is assigned to PAA/PEO miscible blends. From Fig. 3, it is clear that the content of MWNTs at the interface increases with increasing layers.

3.3.2. Electrostatic force microscopy (EFM) analysis

To further explore the composites assembled here, electrostatic force microscopy (EFM) was performed. The dielectric constants of PEO (ε~5.1)[44] and PAA (ε~3)[45] are significantly different, thereby, the presence of multiple phases can be directly elucidated by EFM. First, signals for pure PEO and pure PAA samples were obtained to

Table 1
Comparison of ionic conductivities for systems studied.

	Literature [21]	Two component system	Tri-component system	Literature [21]	Two component system	Tri-component system
Type of film	PEO/PAA	PEO/PAA	PEO/PAA/PEO/(PAA + MWNT)	PEO/PAA	PEO/PAA	PEO/PAA/PEO /(PAA + MWNT)
Number of stacks	30	40	20	30	40	25
Relative humidity	53%	48%–56%	48%–56%	53%	48%–56%	48%–56%
$LiCF_3SO_3$ Conc.	0	0	0	0.1 M	0.1 M	0.1 M
Limiting Ionic conductivity	~10^{-9} S cm^{-1}	~10^{-9} S cm^{-1}	~10^{-8} S cm^{-1}	~10^{-7} S cm^{-1}	~10^{-7} S cm^{-1}	~10^{-6} S cm^{-1}

Samsung Ex. 1016, Page 4 of 8
Samsung Electronics Co., Ltd., et al. v. Molecular Rebar Design, LLC
IPR2025-00358

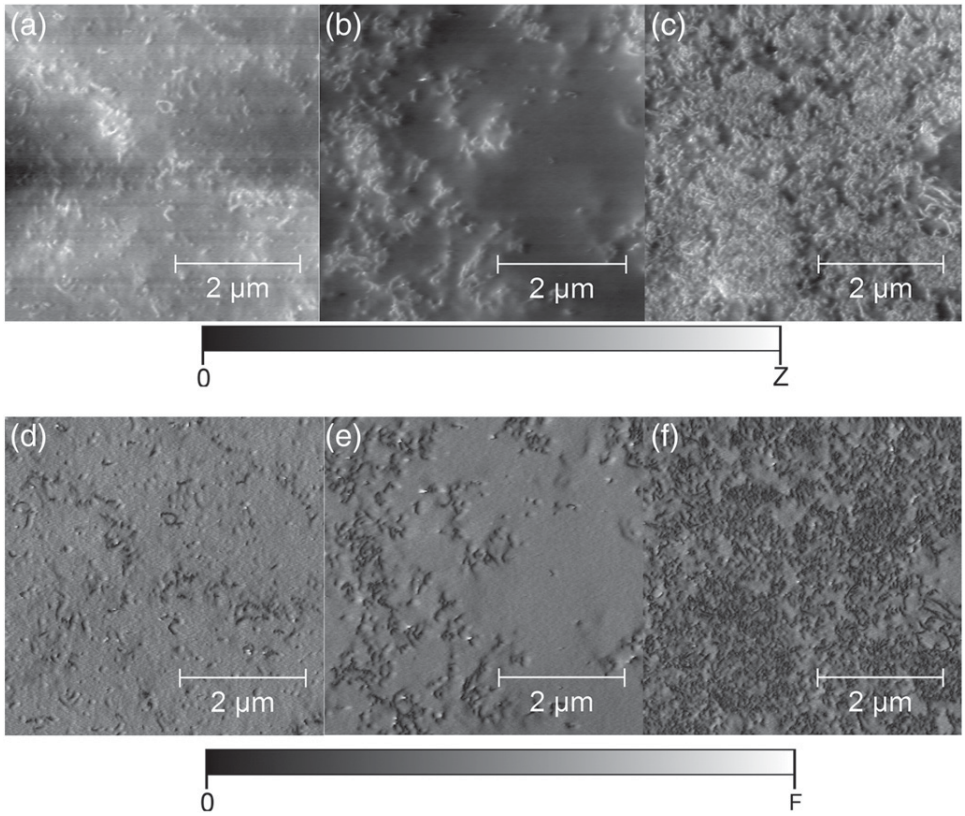

Fig. 3. Topography of (a) [PEO/PAA/PEO/(PAA + MWNT)]$_5$ (Z = 54 nm), (b) [PEO/PAA/PEO/(PAA + MWNT)]$_{10}$ (Z = 76 nm) and (c) [PEO/PAA/PEO/(PAA + MWNT)]$_{25}$ (Z = 43 nm); lateral force image of (d) [PEO/PAA/PEO/(PAA + MWNT)]$_5$ (F = 13.4 nN), (e) [PEO/PAA/PEO/(PAA + MWNT)]$_{10}$ (F = 13.8 nN) and (f) [PEO/PAA/PEO/(PAA + MWNT)]$_{25}$ (F = 13.7 nN).

understand the pure component behavior. Fig. 4(a) provides these pure component measurements, as well as composite curve fitting for the obtained data. It is important to note that the magnitude of the phase shift is arbitrary, only the phase shift difference is of direct importance. As shown, PAA is well fit by a single Gaussian curve with a peak at about 0.50 V, while PEO is well modeled by two peaks, a large peak at 0.73, and a smaller peak at 0.90.

EFM phase images and corresponding peak fitting of [PEO/PAA]$_2$ are presented in Figs. 4(b) and (c). From Fig. 4(b) one can see that the inclusions of PEO and PAA are well-defined in the EFM image and provide the highest contrast. The white region represents high phase shift and the dark region represents low phase shift, which correspond to the high dielectric constant of PEO and low dielectric constant of PAA, respectively. Fig. 4(c) shows that the peak fitting results in three peaks, which, based on relative peak positions, correspond well with a combination of the single peak of PAA, and the two peaks for PEO shown in Fig. 4(a) for the pure component species. In correspondence with our previous work [23], in-plane phase heterogeneity exists in the ultrathin two stack system of [PEO/PAA]$_2$, and this surface is dominated by PEO and PEO rich blends for low stack numbers. Thus, the peaks associated with PEO are more prominent than those associated with PAA. Further, we also showed previously that these are primarily blends of PEO/PAA on the surface, which is not apparent in EFM. This is due to the fact that EFM is strictly sensitive to the surface molecular composition, and does not resolve the presence of the blend.

A significant increase in contrast variation and phase shift in the EFM analysis is obtained for [PEO/PAA/PEO/(PAA + MWNT)]$_{10}$, Fig. 4(d) and (e). As shown in Fig. 4(e), the data are well fit by four peaks: the primary peak associated with PAA, two smaller peaks associated with PEO (the relative positions of which are again in agreement with the pure component measurements above), and a small, but very wide peak, with a maximum at about 1.55 V, as shown in the inset of Fig. 4 (e). Based on reference [23], an equivalent [PEO/PAA] structure would have a surface composition of ~90% PAA, which leads to the conclusion that the PAA peak is most prominent, with a much smaller PEO contributions. The fourth peak may represent the MWNTs themselves, which have high dielectric constants (up to 300) [46].

To confirm that the fourth peak is related to MWNTs, the dielectric constant associated with this phase, ε_3, can be roughly evaluated as per Krayev [32,47] via

$$\frac{\Delta\theta_1-\Delta\theta_2}{\Delta\theta_2-\Delta\theta_3}=\frac{\dfrac{\varepsilon_1{}^2(\varepsilon_1-1)}{(\varepsilon_1+1)^3}-\dfrac{\varepsilon_2{}^2(\varepsilon_2-1)}{(\varepsilon_2+1)^3}}{\dfrac{\varepsilon_2{}^2(\varepsilon_2-1)}{(\varepsilon_2+1)^3}-\dfrac{\varepsilon_3{}^2(\varepsilon_3-1)}{(\varepsilon_3+1)^3}} \tag{2}$$

with knowledge of the dielectric constants and corresponding phase shifts of the other two components (i.e., PEO and PAA with ε_k and $\Delta\theta_k$, k = 1,2, respectively, where the phase shift for PEO is taken as the larger PEO peak) in this tertiary phase system. It is important to note that Eq. (2) was primarily developed for dielectric constants of less than 20 [32]. Thus, the higher values reported here have to be taken with some caution. In the region of the center of the fourth peak, i.e. at $\Delta\theta_3$ = 1.54 V to 1.58 V, Eq. (2) yields a value of 100–400 for ε_3, in reasonable agreement with the dielectric properties of multi-walled carbon nanotubes (ε~300) [46]. The distribution of ranges, the broadness of this apparent peak and the fact that the peak is small relative to the amount of carbon nanotubes observed in Fig. 3 may reflect either a distribution of carbon nanotube orientations on the surface, or the influence of hydrogen bonding

Samsung Ex. 1016, Page 5 of 8
Samsung Electronics Co., Ltd., et al. v. Molecular Rebar Design, LLC
IPR2025-00358

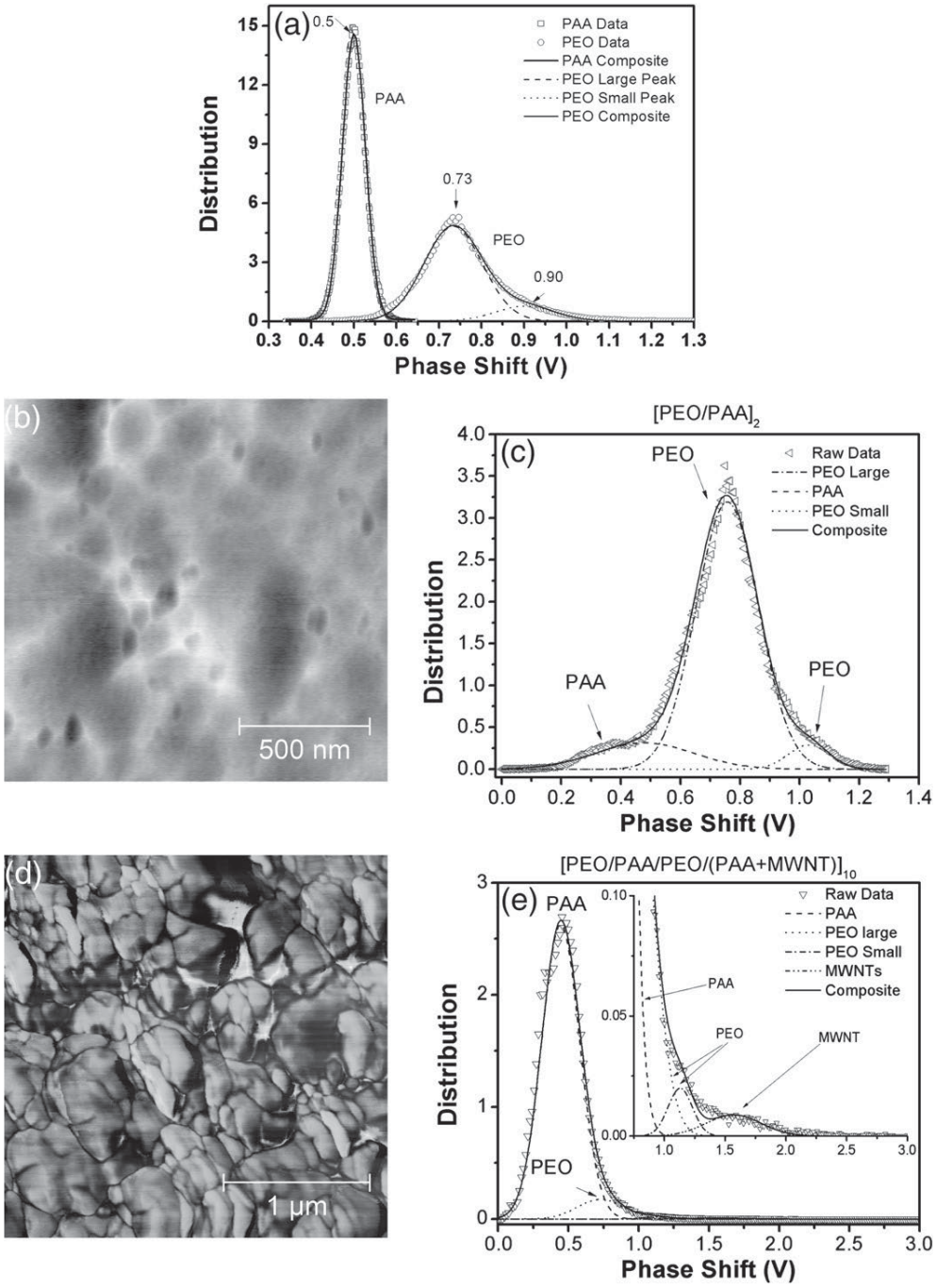

Fig. 4. (a) Phase shift *vs.* distribution based on the EFM image for pure component PEO and PAA samples. (b) EFM phase contrast image of $[PEO/PAA]_2$, (c) Plot of phase shift *vs.* distribution based on the EFM image (b). (d) EFM phase contrast image of $[PEO/PAA/PEO/(PAA+MWNT)]_{10}$, (e) phase shift *vs.* distribution based on the EFM image (d). *Inset:* tail of phase shift *vs.* distribution.

interactions between PAA and the nanotubes, where PAA may effectively be coating the nanotubes, resulting in a PAA dominated EFM signal.

3.3.3. Ion transfer model for LBL films

In light of the conductivity, LFM and EFM data above and our previous work [23], an ion transfer model for $[PEO/PAA]_n$ and $[PEO/PAA/PEO/(PAA+MWNT)]_m$ LBL structures is provided in Fig. 5. From our previous work [23], each $[PEO/PAA]_n$ LBL layer in thick films ($n>10$) was "autoblended", rather than being a pure phase, having a minor component concentration (e.g., PEO in the PAA layer) on the order of ~10 wt.%. However, this value increased to 40 wt.% PEO in the PAA layer for lower stack numbers ($n<\sim5$), and full in-plane heterogeneity with regions of crystalline PEO and bulk-like PAA for $n=2$. As such, we saw strong ionic conductivity increases with decreasing stack numbers as PEO concentration in the (otherwise poorly conductive) PAA layer increased. These results are reflected in the model in Fig. 5(a), which shows ion conductivity occurs readily through the

Samsung Ex. 1016, Page 6 of 8
Samsung Electronics Co., Ltd., et al. v. Molecular Rebar Design, LLC
IPR2025-00358

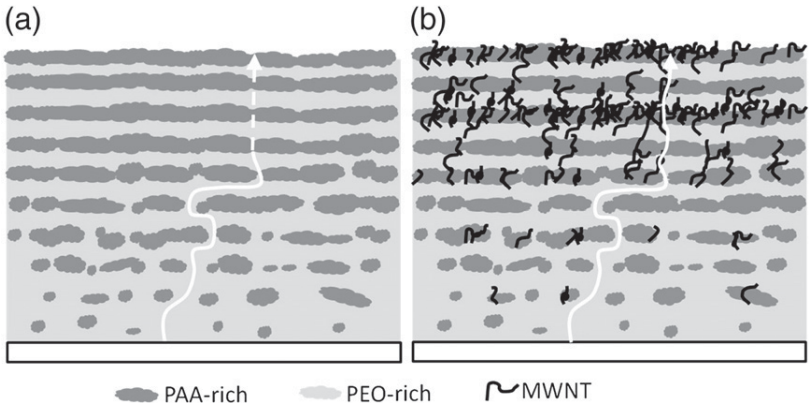

Fig. 5. Ion transfer model for two LBL systems, (a) [PEO/PAA]n system (b) [PEO/PAA/PEO/(PAA + MWNT)]m system; white line represents ion transfer path.

PEO rich layer until the PAA-rich layer is fully formed for higher stack numbers, where the limiting conductivity is reached (as indicated by the dashed white line). In the present work, even systems where Li Trif was added, Fig. 2(b), though they showed improved conductivity of about two orders relative to $[PEO/PAA]_n$, still exhibited a loss in conductivity with increasing stack number due to the PAA rich blend dominating the surface, indicating that the same mechanism is in effect.

The ionic conductivity mechanism of tri-component LBL films is provided in Fig. 5(b). In an analogous way to the $[PEO/PAA]_n$ system, the high ionic conductivity observed for $[PEO/PAA/PEO/(PAA + MWNT)]_m$ is obtained due to a PEO-rich path in ultrathin LBL films (low stack numbers). Improved limiting conductivity in $[PEO/PAA/PEO/(PAA + MWNT)]_m$ systems must be due to the presence of the MWNTs. Modified MWNTs diffuse towards the PEO-PAA interface due to the tendency of their carboxylic acid moieties to act as hydrogen bond donors with PEO, resulting in MWNTs which take up residence near the interface. This is supported in recent studies involving hydrogen bonding of COOH modified CNTs in PAH [40], PEI [30] and CNT-NH_2 [41]-based systems.

The presence of MWNTs at the interface may result in improved conductivity due to either (i) improved interpenetration of PEO and/or MWNTs into the relatively poorly conducting PAA regions or (ii) improved ionic transport due to the MWNTs themselves. Data in Fig. 2(a) suggest that (i) does occur, since there is an improvement in limiting conductivity without the addition of Li Trif to the system. Such phase mixing is likely to occur during the dipping process, where the temporarily exposed interfacial region between the already deposited PEO film and the added PAA + MWNT film is highly mobile [48]. MWNTs provide improved surface area for phase mixing, resulting in improved PEO penetration into the PAA rich phase. In addition, MWNTs may further suppress crystallinity of PEO. For example, Tirtha et al. [49] found the melting temperature and the extent of crystallinity of PEO crystals decreased with increasing SWNT, which resulted in a higher conductivity. Further, interpenetration may take the form of MWNTs spanning whole bilayers. Based on the data provided in Fig. 1, the bilayer stack thickness (i.e., one PEO/PAA stack, or $n = m/2$) is on the order of 40–60 nm. Clearly the carbon nanotubes observed in Fig. 3 are much longer than this, so, if there is sufficient mobility during the dipping process, MWNTs may penetrate into the PAA layers deposited without MWNTs.

Further, data in Fig. 2(b) suggests that the second point mentioned above also occurs due to the fact that very little change in conductivity as a function of the stack number was observed for $[PEO/PAA/PEO/(PAA + MWNT)]_m$ systems where Li Trif was added. It is known that the charge carrier (Li^+) concentration increases with MWNTs as Li^+ ions prefer adsorbing at the walls of the MWNTs [43]. Similar phenomena were also observed for single walled nanotubes, where Li diffusion to the interior of SWNTs occurred through open ends and sidewall defects [50]. Thus, the blended film structure of incorporated MWNT may provide a pathway for both improved ion transfer through the polymer matrix and intra-MWNT ion transport unhindered by the otherwise poorly conductive PAA, yielding PAA-rich films with high ionic conductivity.

4. Conclusions and outlook

Along with the improved growth rate compared with other LBL films containing CNTs, the [PEO/PAA/PEO/(PAA + MWNT)] assembly provided ionic conductivity clearly superior to that of $[PEO/PAA]_n$ films. $[PEO/PAA/PEO/(PAA + MWNT)]_m$ LBL films provide thickness-normalized ionic conductivity values of $10^{-5}\,S\,cm^{-1}$ for ultrathin films and $10^{-8}\,S\,cm^{-1}$ for undoped bulk films, while the corresponding values for $[PEO/PAA]_n$ films are $10^{-7}\,S\,cm^{-1}$ and $10^{-9}\,S\,cm^{-1}$. EFM results show that PEO dominates the surface for low stack numbers, while PAA dominates for higher stack numbers. PAA dominated layers effectively act as a barrier to transport due to the fact that PAA is a poor electrolyte compared with PEO, therefore both types of films show strongly limiting conductivity for high stack numbers. However, in the presence of lithium triflate dopant, the tri-component (MWNT) system shows relatively stable ionic conductivity on the order of $10^{-5}\,S\,cm^{-1}$ over a broad range of thicknesses.

Enhancement in ionic conductivity from MWNTs is attributed to both improved interpenetration of MWNTs and PEO into the relatively poorly conducting PAA regions and improved ionic transport within MWNTs themselves. The former is evidenced by the presence of MWNTs at the PAA free surface measured using LFM. The latter is supported by the fact that, in Li Trif doped $[PEO/PAA/PEO/(PAA + MWNT)]_m$ assemblies, only a modest decrease in conductivity with increasing thickness was observed, indicating that the carbon nanotubes promote effective adsorption sites for the lithium ions within the interfacial region of PEO and PAA. The high ionic conductivity and good interfacial compatibility with lithium triflate indicates that the tri-component LBL film electrolytes are promising candidates for use in solid state rechargeable lithium ion batteries

In the ultrathin regime, the MWNTs did not seem to boost overall conductivity in the presence of Li Trif to the same degree as systems without Li Trif. Given the above understanding of film deposition and influence of MWNT, future work on this system should focus on how to maintain the high conductivity achieved in the ultrathin film (low m) region for bulk systems lacking dopants, and translate that to direct improvement in dopant containing samples.

Samsung Ex. 1016, Page 7 of 8
Samsung Electronics Co., Ltd., et al. v. Molecular Rebar Design, LLC
IPR2025-00358

Acknowledgments

We acknowledge Orb Acton and Prof. A. K.-Y. Jen's group for assistance in the gold deposition and impedance measurements, and Cheaptubes, Inc., and Thin Film Devices, Inc. for providing MWNT samples and ITO substrate materials, respectively. Xianke Gu thanks the China Scholarship Council for its fellowship support. D.B. Knorr thanks ARCS for a graduate fellowship.

References

[1] J.M. Tarascon, M. Armand, Nature 414 (2001) 359.
[2] M. Park, X.C. Zhang, M.D. Chung, G.B. Less, A.M. Sastry, J. Power Sources 195 (2010) 7904.
[3] R.C. Agrawal, G.P. Pandey, J. Phys. D: Appl. Phys. 41 (2008) 223001.
[4] J.M. Tarascon, A.S. Gozdz, C. Schmutz, F. Shokoohi, P.C. Warren, Solid State Ionics 86–88 (1996) 49.
[5] S. Zhou, D. Kim, Polym. Adv. Technol. 21 (2010) 797.
[6] X.J. Wang, J.J. Kang, Y.P. Wu, S.B. Fang, Electrochem. Commun. 5 (2003) 1025.
[7] Z.Y. Wen, T. Itoh, T. Uno, M. Kubo, T.L. Wen, O. Yamamoto, Solid State Ionics 175 (2004) 739.
[8] M.J. Reddy, J.S. Kumar, U.V.S. Rao, P.P. Chu, Solid State Ionics 177 (2006) 253.
[9] R. Baskaran, S. Selvasekarapandian, N. Kuwata, Solid State Ionics 177 (2006) 2679.
[10] J.Y. Xi, X.P. Qiu, J. Li, X.Z. Tang, W.T. Zhu, L.Q. Chen, J. Power Sources 157 (2006) 501.
[11] H. Pitawala, M. Dissanayake, V.A. Seneviratne, Solid State Ionics 178 (2007) 885.
[12] S. Kim, S.J. Park, Solid State Ionics 178 (2007) 973.
[13] J.Y. Xi, S.J. Miao, X.Z. Tang, Macromolecules 37 (2004) 8592.
[14] C. Capiglia, P. Mustarelli, E. Quartarone, C. Tomasi, A. Magistris, Solid State Ionics 118 (1999) 73.
[15] Z. Gadjourova, Y.G. Andreev, D.P. Tunstall, P.G. Bruce, Nature 412 (2001) 520.
[16] H. Schonherr, C.W. Frank, Macromolecules 36 (2003) 1199.
[17] M.V. Massa, K. Dalnoki-Veress, J.A. Forrest, Eur. Phys. J. E. 11 (2003) 191.
[18] H. Wang, J.K. Keum, A. Hiltner, E. Baer, B. Freemann, A. Rozanski, A. Galeski, Science 323 (2009) 757.
[19] D.M. DeLongchamp, P.T. Hammond, Langmuir 20 (2004) 5403.
[20] J.L. Lutkenhaus, K.D. Hrabak, K. McEnnis, P.T. Hammond, J. Am. Chem. Soc. 127 (2005) 17228.
[21] J.L. Lutkenhaus, K. McEnnis, P.T. Hammond, Macromolecules 40 (2007) 8367.
[22] J.R. Maccallum, M.J. Smith, C.A. Vincent, Solid State Ionics 11 (1984) 307.
[23] X. Gu, D.B. Knorr, G. Wang, R.M. Overney, Thin Solid Films 519 (2011) 5955.
[24] Y.X. Li, J.A. Yerian, S.A. Khan, P.S. Fedkiw, J. Power Sources 161 (2006) 1288.
[25] M.K. Shin, Y.J. Kim, S.I. Kim, S.K. Kim, H. Lee, G.M. Spinks, S.J. Kim, Sens. Actuators, B 134 (2008) 122.
[26] S.S. Ojha, D.R. Stevens, K. Stano, T. Hoffman, L.I. Clarke, R.E. Gorga, Macromolecules 41 (2008) 2509.
[27] K. Awasthi, S. Awasthi, A. Srivastava, R. Kamalakaran, S. Talapatra, P.M. Ajayan, O.N. Srivastava, Nanotechnology 17 (2006) 5417.
[28] J.H. Ahn, Y.J. Kim, C.X. Wang, Met. Mater. Int. 12 (2006) 69.
[29] H. Paloniemi, M. Lukkarinen, T. Aaritalo, S. Areva, J. Leiro, M. Heinonen, K. Haapakka, J. Lukkari, Langmuir 22 (2006) 74.
[30] A.A. Mamedov, N.A. Kotov, M. Prato, D.M. Guldi, J.P. Wicksted, A. Hirsch, Nat. Mater. 1 (2002) 190.
[31] T. Farhat, G. Yassin, S.T. Dubas, J.B. Schlenoff, Langmuir 15 (1999) 6621.
[32] A. Krayev, R. Talroze, Polymer 45 (2004) 8195.
[33] E. Meyer, L. Howald, R.M. Overney, H. Heinzelmann, J. Frommer, H.J. Guntherodt, T. Wagner, H. Schier, S. Roth, Nature 349 (1991) 398.
[34] C. Buenviaje, S.R. Ge, M. Rafailovich, J. Sokolov, J.M. Drake, R.M. Overney, Langmuir 15 (1999) 6446.
[35] D.M. DeLongchamp, P.T. Hammond, Chem. Mater. 15 (2003) 1165.
[36] S. Lanfredi, J. Appl. Phys. 86 (1999) 2215.
[37] P. Podsiadlo, M. Michel, J. Lee, E. Verploegen, N.W.S. Kam, V. Ball, J. Lee, Y. Qi, A.J. Hart, P.T. Hammond, N.A. Kotov, Nano Lett. 8 (2008) 1762.
[38] C. Porcel, P. Lavalle, V. Ball, G. Decher, B. Senger, J.C. Voegel, P. Schaaf, Langmuir 22 (2006) 4376.
[39] B.S. Shim, Z.Y. Tang, M.P. Morabito, A. Agarwal, H.P. Hong, N.A. Kotov, Chem. Mater. 19 (2007) 5467.
[40] P.V. Pavoor, B.P. Gearing, R.E. Gorga, A. Bellare, R.E. Cohen, J. Appl. Polym. Sci. 92 (2004) 439.
[41] S.W. Lee, B.S. Kim, S. Chen, Y. Shao-Horn, P.T. Hammond, J. Am. Chem. Soc. 131 (2009) 671.
[42] W.H. Meyer, Adv. Mater. 10 (1998) 439.
[43] E. Frackowiak, S. Gautier, H. Gaucher, S. Bonnamy, F. Beguin, Carbon 37 (1999) 61.
[44] C. Fanggao, G.A. Saunders, E.F. Lambson, R.N. Hampton, G. Carini, G. DiMarco, M. Lanza, J. Polym. Sci. Part B: Polym. Phys. 34 (1996) 425.
[45] S. Tamburic, D.Q.M. Craig, J. Controlled Release 37 (1995) 59.
[46] L. Wang, Z.M. Dang, Appl. Phys. Lett. 87 (2005) 042903.
[47] A.V. Krayev, G.A. Shandryuk, L.N. Grigorov, R.V. Talroze, Macromol. Chem. Phys. 207 (2006) 966.
[48] M. Olek, J. Ostrander, S. Jurga, H. Mohwald, N. Kotov, K. Kempa, M. Giersig, Nano Lett. 4 (2004) 1889.
[49] T. Chatterjee, K. Yurekli, V.G. Hadjiev, R. Krishnamoorti, Adv. Funct. Mater. 15 (2005) 1832.
[50] H. Shimoda, B. Gao, X.P. Tang, A. Kleinhammes, L. Fleming, Y. Wu, O. Zhou, Phys. Rev. Lett. 88 (2001) 15502.

Samsung Ex. 1016, Page 8 of 8
Samsung Electronics Co., Ltd., et al. v. Molecular Rebar Design, LLC
IPR2025-00358